Journal of Materials Chemistry A

Accepted Manuscript

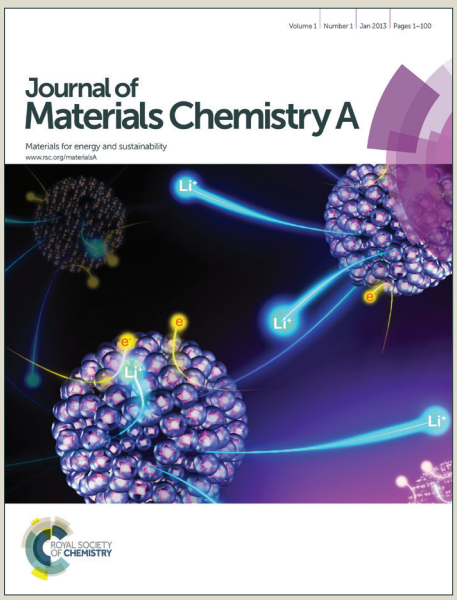

ROYAL SOCIETY OF CHEMISTRY

www.rsc.org/materialsA

3D conductive network based free-standing PANI-RGO-MWNTs hybrid film for high-performance flexible supercapacitor

Haosen Fan[a, b], Ning Zhao[b*], Hao Wang[b], Jian Xu[b*] and Feng Pan[a*]

Received (in XXX, XXX) Xth XXXXXXXXX 20XX, Accepted Xth XXXXXXXXX 20XX
First published on the web Xth XXXXXXXXX 20XX
DOI: 10.1039/b000000x

A facile method was successfully conducted to construct 3D conductive network based free-standing polyaniline/reduced graphene oxide/carbon nanotube ternary hybrid film, in which 3D conductive network was synergistically assembled by MWNTs and GO. The synergistical assembly of carbon nanotubes and graphene oxide not only increase the basal spacing between graphene sheets but also effectively bridge the defects of reduced graphene oxide to form 3D conductive network. Due to the 3D conductive network with high conductivity and the synergistic effect of polyaniline with carbon nanotubes and graphene, the as-prepared ternary hybrid film possessed high specific capacitance and good cycle stability as flexible supercapacitor electrode. This study gives a better insight for the preparation of functional flexible hybrid film by combining conducting polymer with different dimensional carbon materials.

Introduction

With the growing concerns over the finite fossil-fuel supplies and environmental issues, the development of alternative energy conversion/storage resources is very important and indispensable.[1] Supercapacitors, also called electrochemical capacitors, are likely to play an important role in energy storage due to theirs high power density, long cycle life and many potential applications in portable electronic devices, hybrid electric vehicles and implantable medical devices.[2, 3] Recently, there has been increasing interest in flexible supercapacitors as energy storage devices to meet the various requirements of modern applications.[4, 5] An ideal flexible supercapacitor should have a combination of good flexibility with excellent mechanical strength and large electrochemical behavior.[6] Although conducting polymers and transition metal oxides have been widely studied as supercapacitors due to their prominent capacitive properties, only carbon materials (carbon fibers,[7, 8] carbon nanotubes[9, 10] and graphene[11, 12]) have displayed favorable flexibility and hence been promising as freestanding and flexible capacitor.

Recently, graphene sheet, a two-dimensional all-sp^2-hybridized carbon, is proposed as one of the ideal candidates for the next generation flexible electrode materials, due not only to its structural, mechanical and electrical properties, but also to its high accessible surface area (2630 m^2 g^{-1}).[13] In general, graphene or graphene oxide sheets are often combined with polyaniline (PANI) to improve the capacitance property of flexible film because of the specially synergistic effect of PANI and graphene or graphene oxide sheets. It is well known that PANI is one of the most promising conducting polymers showing high capacitance, the good environmental stability and easy of preparation. PANI materials have been widely studied to promote the electrochemical capacitance of flexible CNT and graphene papers.[14, 15] However, previous reports indicate that the actual performance of graphene-based materials is much lower than the anticipated value (estimated from the ultrahigh surface area of graphene) due to facile aggregation of graphene during preparation, attributing to facile restacking of reduced graphene oxide because of strong Vander Waals interactions among individual graphene.[16] Fortunately, the combination of carbon nanotubes and graphene have been demonstrated to improve the capacitor property of graphene with the existence of carbon nanotubes which are believed to increase the basal spacing between graphene sheets, as well as to bridge the defects for electron transfer.[17-19] Therefore, the inclusion of carbon nanotubes is expected to improve the unique potential of graphene film as a freestanding electrode for supercapacitors.

Herein, we demonstrate the preparation of a hierarchical flexible polyaniline/reduced graphene oxide/carbon nanotube ternary film based on 3D conductive network by introducing carbon nanotubes into graphene system, which is prepared by a rapid mixture polymerization of aniline monomers in the presence of flexible graphene oxide/carbon nanotube composite film. This novel flexible film exhibits excellent electrochemical performance due to the high electrical conductivity of 3D conductive network and extraordinary architecture, which can effectively combine both the faradaic capacitance and double-layer capacitance at the electrode-electrolyte interfaces. the as-prepared ternary flexible film show high specific capacitance in 1 M H_2SO_4 aqueous solution, showing promising application in flexible supercapacitors.

Experimental

Materials

Aniline (ANI, Beijing Chemical Co.) was distilled under reduced pressure. Ammonium persulfate (APS, Sinopharm Chemical Reagent Co.), graphite (Alfa Aesar, 325 mesh), commercial multiwall carbon nanotubes (MWNTs, 10-30 nm in diameter, 5-15 μm in length, purity ≥ 95 wt %, Shenzhen Nanotech Port Co., Ltd.), and other reagents were all A. R. grade and used without further treatment.

Preparation of PANI-RGO-MWNTs hybrid film

Firstly, 50 mg graphene oxide (GO, prepared by the modified Hummers method[20]) was dispersed in distilled water (50mL) by ultrasonic treatment for 30 min. MWNTs (50 mg) were added and then sonicated for another 30 min. The resulting

complex dispersion was filtered by a vacuum filter equipped with a 0.45 μm porous PTFE membrane to produce a MWNTs-GO film. Secondly, PANI and MWNTs-GO hybrid film was performed by a typical rapid mixture polymerization. Aniline (1 mmol) was dissolved in 50mL of 1 M $HClO_4$ solution and APS (1mmol) was dissolved in 20 mL of the same $HClO_4$ solution. The two solutions were then rapidly poured together and immediately stirred to ensure sufficient mixing before the polymerization began. After being stirred strongly for 1 min, the solution was stopped stirring and the MWNTs-GO film was carefully immersed into it. Reactions were carried out at room temperature for 12 h without stirring. The obtained PANI-GO-MWNTs film was rinsed with distilled water several times. Thirdly, the PANI-GO-MWNTs film was reduced by 55% hydroiodic acid for 1 h at 100 °C[21] and the final PANI-RGO-MWNTs ternary composite film was obtained.

Electrochemical measurements

Electrochemical performances of all samples were measured with a three electrode system, in which platinum foils and saturated calomel electrode (SCE) were used as counter and reference electrodes, respectively. The electrolyte is 6M KOH aqueous solution. Cyclic voltammetry (CV) and electrochemical impedance spectroscopy (EIS) measurements were performed by using a Zahner IM6 electrochemical working station. The scan voltage ranged from -1.0 to 0 V in the CV measurements.

Characterization

Morphology of all products was characterized by scanning electron microscope (SEM, Hitachi S4800) and transmission electron microscope (TEM, JEOL JEM-2200FS), respectively. Fourier transform infrared (FTIR) spectra were recorded on a Bruker Equinox 55 spectrometer in the range of 400-4000 cm^{-1} at room temperature. X-ray photoelectron spectroscopy (XPS) analysis was carried out on an ESCALab220i-XL electron spectrometer from VG Scientific. Al-Kα radiation was used as the X-ray source and operated at 300W.

Results and Discussion

As the scheme summarized in Fig. 1a, a simple strategy is designed to improve the capacitive performances by introducing MWNTs into GO and then combining with PANI. GO and MWNTs mixture firstly is dispersed in aqueous media by ultrasonication and prepare a GO-MWNTs film by filtration of the diluted dispersion. In this procedure, the long and tortuous MWNTs are embeded between the GO layers to play an important role in inhibiting the aggregation of 2D GO, which will effectively increase the contact surface area with electrolyte. That is, the incorporation of MWNTs embeded between GO layers will not only provide open channels for the ionic transport and reduced ionic diffusion length by preventing the aggregation of graphene but also be able to bridge the gaps between reduced GO to form a three dimensional conductive network, which provide an efficiently conductive pathways for electron conduction in ternary film. After a rapid-mixture polymerization of aniline in the presence of GO-MWNTs film and reduction the GO in hydroiodic acid, as shown in Fig. 1b, the final PANI-MWNTs-graphene ternary composite film was successfully prepared with sandwich structure of stacked layers. As a result, owing to a 3D conductive network as the supported skeleton and the synergistic effect of polyaniline with carbon nanotubes and graphene, a ternary flexible electrode material with improved capacitive performance of high specific capacitance can be anticipated by designing hierarchical PANI-RGO-MWNTs architecture.

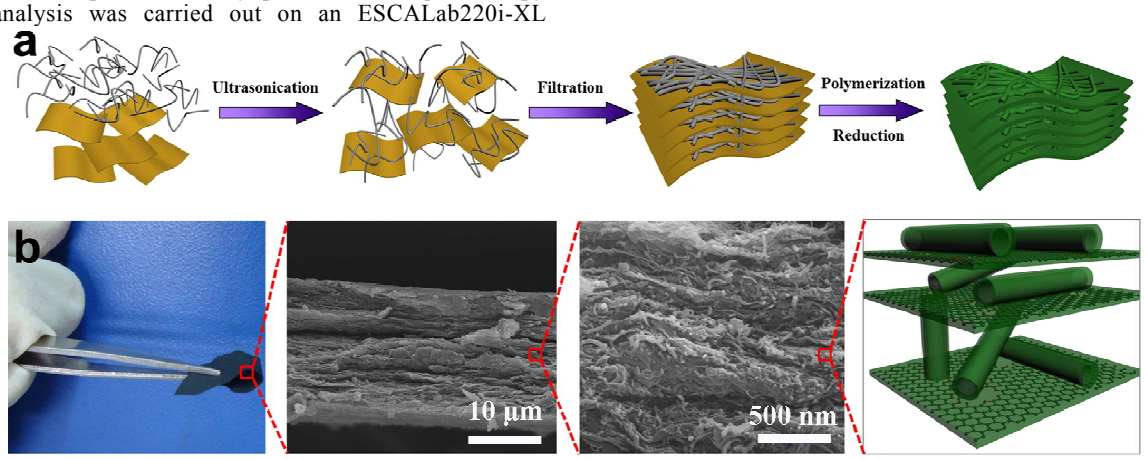

Fig. 1 Schematic illustration of the formation of flexible PANI-RGO-MWNTs ternary hybrid film.

Fig. 2 shows the the aqueous dispersibility of GO, MWNTs and GO-MWNTs. It is well known that GO sheets can be formed as well-dispersed aqueous colloids by ultrasonic dispersion. Unfortunately, GO sheets are still apt to aggregate together after keeping stationary for a day. This is mainly due to facile restacking of GO sheets by Vander Waals forces. The MWNTs show the poor dispersion because most of the MWNTs deposite at the bottom after stopping ultrasonication for 5 minutes. However, the GO-MWNTs dispersion exhibits strong metallic luster solution and good dispersibility due to inserting MWNTs into the interlayer of GO sheets. Hence, the purpose of mutual dispersion of MWNTs and GO are achieved by the ultrasonic dispersion of their mixture solution. Note that the good GO-MWNTs dispersion liquid can keep for a month in staitionary state without any deposition.

It is observed that the filtration of the aqueous GO dispersion through a cellulose membrane filter yielded, after vacuum drying, a brown, free-standing and flexible GO film

Fig. 2 Digital camera images of the aqueous dispersibility of GO, MWNTs and GO-MWNTs.

(Figure 3a). The GO film can be easily rolled up on a glass rod (Inset of 3a). GO-MWNTs film is obtained by the same filtration method, also showing flexible property, but the color of the film is a litter bit difference to show black with a obvious metallic luster (Figure 3b and inset). The thickness of the film can be adjusted by the concentration and volume of GO or GO-MWNTs aqueous dispersion. After polymerization, the PANI layer was coated on the surface of GO and embeded between GO-MWNTs layers to generate PANI-GO-MWNTs film, which maintained the original integrity to have good flexibility (Figure 3c, and Insets). The PANI-RGO-MWNTs,which was reduced from PANI-GO-MWNTs, also maintained good flexibility (Figure 3d, and Insets). To be similar to GO and GO-MWNTs hybrid films,the PANI-GO/RGO-MWNTs films with the thickness controllable can be rolled up or bent easily without cracking, which is surely beneficial to its practical applications in flexible electrode materials. Hence, the rapid-mixture polymerization, in which the PANI was grown on the GO sufaces and between GO-MWNTs layers to generate the flexible films, exhibits great advantages of quite simple and large area preparation. Meanwhile, PANI coatings are facilely obtained and controlled with the high specific surface area, and keep the flexibility of the pristine GO-MWNTs film.

Fig. 4a and d show the cross-section and surface SEM images of GO-MWNTs film. The fracture edges of the film image exhibit a layered structure with well-compact layer-by-layer alternate stacking of GO and MWNTs through almost the entire cross-section. MWNTs are uniformly sandwiched between the GO sheets. Surface SEM and high-resolution SEM images (Fig. 4d) reveal that the surfaces of the GO-MWNTs film is quite smooth with GO sheets coating on MWNTs. After a rapid-mixture polymerization of aniline and reduction the GO by hydroiodic acid, the cross-section SEM images of PANI-GO-MWNTs (Fig. 4b) and PANI-RGO-MWNTs (Fig. 4c) films illustrate that they still keep the layer-by-layer structure of the GO-MWNTs, with the exception of the coating of PANI. As is shown from the surface images of PANI-GO-MWNTs (Fig. 4e) and PANI-RGO-MWNTs (Fig. 4f) films, they are both rough enough with many nanoscale protuberance, indicating the

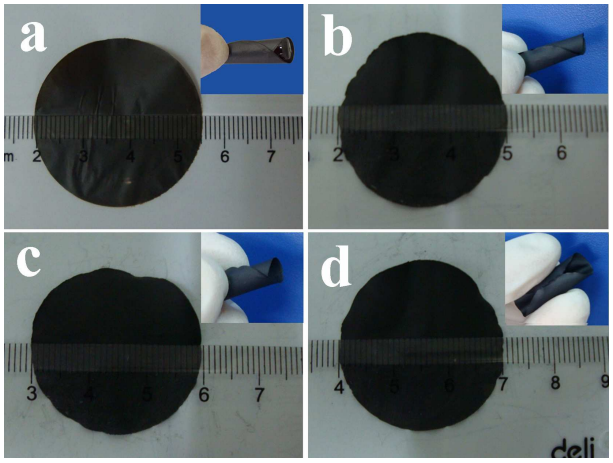

Fig. 3 Digital camera images of flexible films (a) GO (b) GO-MWNTs, (c) PANI-GO-MWNTs, and (d) PANI-RGO-MWNTs. (The inset images indicate the flexibility of the samples).

combination of PANI with GO and MWNTs. As we know, many oxygen-containing functional group such us carboxylic and phenolic hydroxyl groups exist on the surface and edge of GO sheets. In our rapid-mixture polymerization process, after immersing the GO-MWNTs film into reaction system, the functional groups may act as active sites by preferentially adsorbing aniliniumions though electrostatic force. Thus, these sites will act as the seeding dots to attach the polymerization of PANI on the surface of GO and between the GO-MWNTs layers to form PANI nanoparticles and PANI coatings.

Fig. 5 presents TEM images of the broken films by ultrasonic treatment. It is important to note that ultrasonic treatment cannot completely destroy film into a single-layer GO and MWNTs, but into a close-packed structure. As showed in Fig. 5(a, b), it can be found that MWNTs are randomly distributed into the GO sheet by connecting to each other, forming a sandwich structure. After polymerization of aniline (Figure 5c, d), core-shell nanostructures with thin PANI layer coated on MWNTs are formed (black arrow), as well as PANI nanoparticles on the surface of GO (white arrow). As we known, MWNTs used here are not treated by inorganic acid. The π-π stacking force between the graphitic structures of MWNTs and the aromatic rings of PANI is conducive to polymerization PANI layer on the surface of MWNTs. Meanwhile, except for PANI nanoparticles formed in GO oxided site by electrostatic force, the π-π stacking force between PANI and GO is also contribued to PANI layer on the unoxided parts of GO, obtaining a sandwich structured PANI-GO. After reduction of GO, as shown in Fig. 5e and 5f, the coaxial structure of PANI-MWNTs and PANI-RGO is retentive, implying that the reduction process hold on the same structure in the PANI-RGO-MWNTs film. Here, it is worth noting that ultrasonic treatment is not fully destroyed the layer-by-layer structured of three hybrid films so as to show the massive structure in TEM images, rather than a sigle or few layers GO.

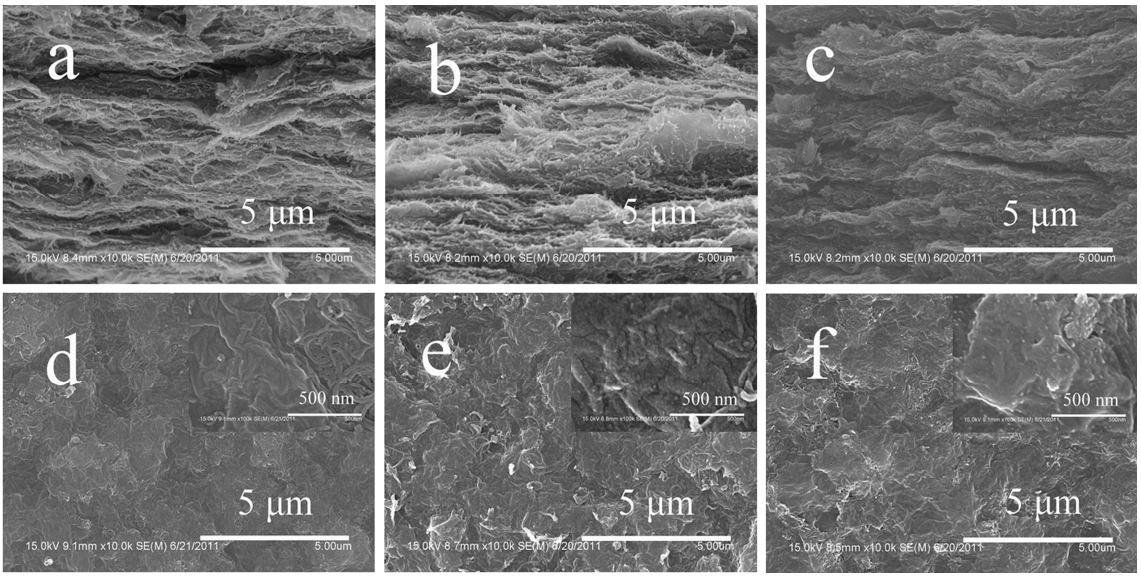

Fig. 4 Cross-section and surface SEM images of GO-MWNTs film (a, d), PANI -GO-MWNTs film (b, e) and PANI -RGO-MWNTs film (c, f). (Insets show high resolution surface SEM images)

The typical FT-IR spectra of all samples are shown in Fig. 6a. MWNTs shows no obvious absorption peak. In comparison to pristine MWNTs, GO-MWNTs shows similar characteristic peaks around 3399, 1729 and 1391-1060 cm^{-1}, which can be attributed to the O-H, C=O in COOH, and C-O in C-OH/C-O-C functional groups, respectively.[22] The resulting PANI-RGO-MWNTs film exhibits similar specific peaks as compared to the peaks of pure PANI. The main transmission bands centered at 1566 and 1486 cm^{-1} are attributed to C=C stretching vibration of quinoid ring and benzenoid ring in PANI chains, indicating the presence of emeraldine salt state of PANI. The peaks at 1298, 1246, 1146 and 818 cm^{-1} are attributed to the following vibrations: C-N stretching vibration of the benzene ring, stretching vibration of the $CN^{\bullet+}$ in the polaron structure of PANI, stretching of C=N (-N=quinoid=N-) and out of plane bending vibration of C-H in benzene ring, respectively.[23]

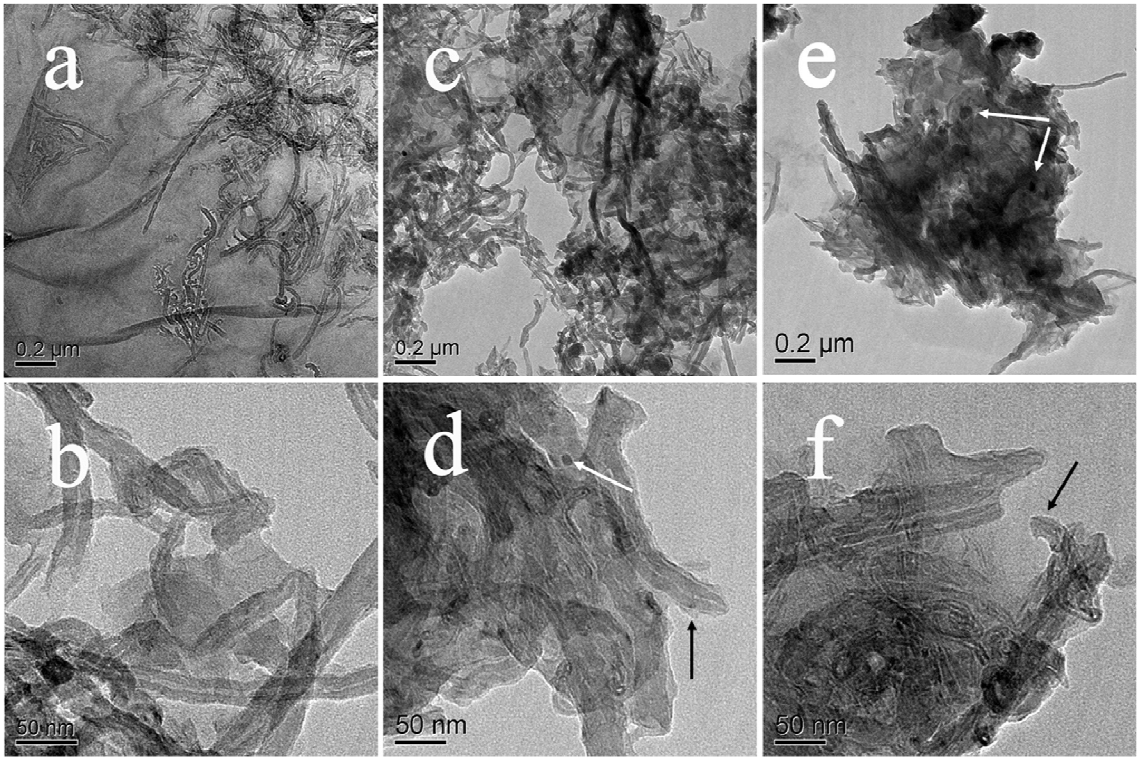

Fig. 5 TEM images of GO-MWNTs film (a, b), PANI-MWNTs-GO film (c, d) and PANI-GRO-MWNTs film (e, f).

Fig. 6b shows the XRD patterns of GO-MWNTs, GO and PANI-RGO-MWNTs. The typical peaks of GO-MWNTs centered at 2θ = 26.1° is corresponds to the (002) interplanar spacing between the MWNTs walls. For pure PANI, the crystalline peaks centered at about 20° and 26° can be assigned to (020) and (200) reflections of PANI, suggesting in its emeraldine salt form.[25] The XRD patterns of PANI-RGO-MWNTs exhibits similar crystal peaks compared with that of PANI, revealing no additional crystalline order is introduced into the obtained ternary hybrid film in the presence of RGO and MWNTs.

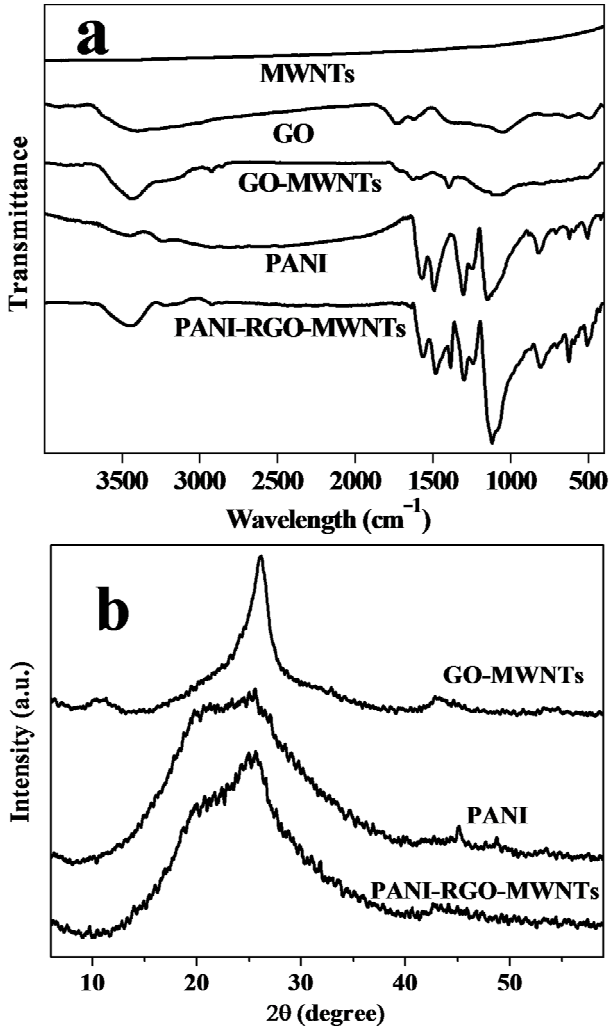

Fig. 6 FTIR and XRD spectra of the obtained examples.

XPS (Fig. 7a) is used to measure the elemental composition on the surface. The survey spectrum shows that GO-MWNTs consists of oxygen (531 eV) and carbon (285 eV). PANI-GO-MWNTs displays additional nitrogen group (399 eV) by the PANI coating on the surface of GO and MWNTs. After the reduction of PANI-GO-MWNTs, The O element content decreases due to the removal of oxygenous functional group in the GO. From the C 1s spectrum of GO in Figure 7b, GO shows the highest hetero-carbon with four components that correspond to carbon atoms in different functional groups: the nonoxygenated ring C (284.9 eV), the C atom in C-O bond (286.2 eV), the carbonyl C (287.8 eV), and the carboxylate carbon (O-C=O) (289.0 eV). These functional groups can be effectively removed by HI reduction based on the significant decrease of hetero-carbon components from the comparison of C 1s spectra between Figure 7b and 7c. After HI reduction, Although the C1s XPS spectrum of the RGO also exhibits these same oxygen groups as compared to the C1s spectrum of GO, their peak intensities are much smaller than those in GO. the percentage of C=C bond in the composite increases from 53.6 to 82.4%, revealing remarkable restoration of the graphitic structure of RGO through the HI reduction. All the above results clearly reveal that GO is successfully reduced to RGO in this simple HI reduction method.

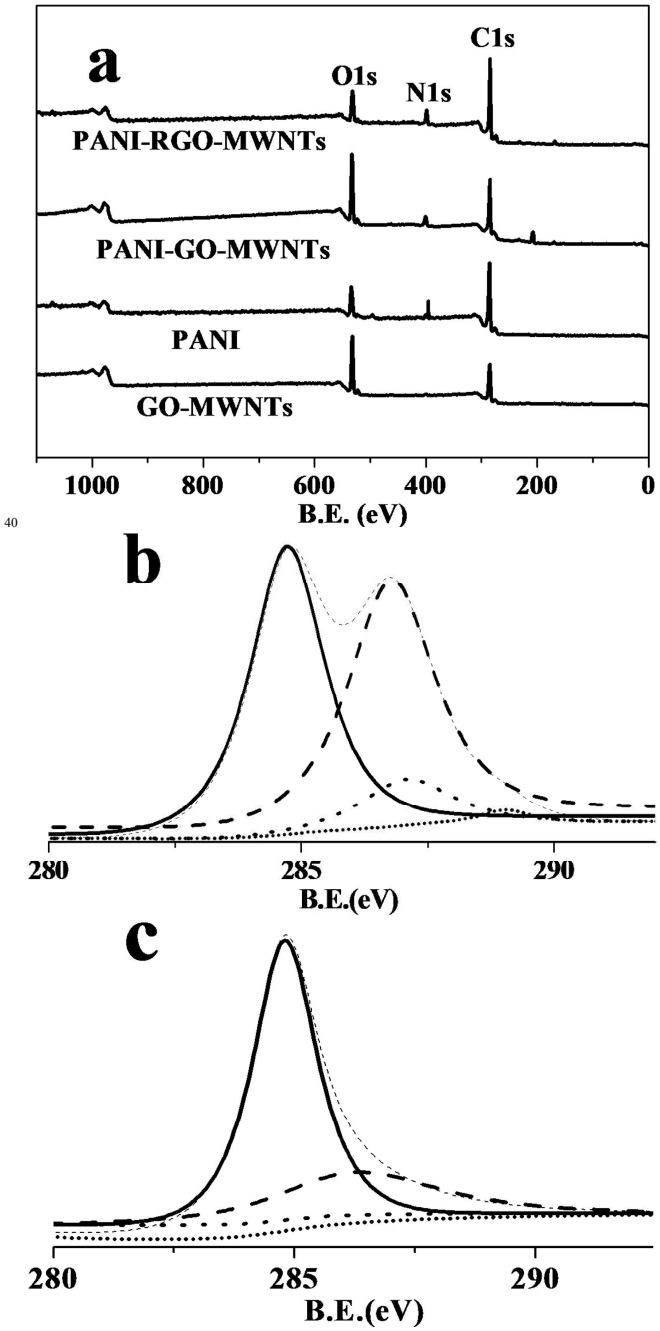

Fig. 7 XPS spectra of all examples (a). C1s spectra of (b) GO and (c) RGO.

The electrochemical performance of the flexible film samples were characterized by cyclic voltammograms (CV) and electrochemical impedance spectroscopy (EIS). Fig. 8a exhibits the CV curves of all examples at a sweep rate of 5 mV s^{-1} with the potential range from -0.2 to 0.8 V in 1 M H_2SO_4 solution. For PANI-RGO-MWNTs and PANI-GO-MWNTs electrodes, the two couples of redox peaks ($C_1/A_1$and C_2/A_2) in CV curves result in the redox capacitance. Redox peaks (C_1/A_1) are attributed to the redox transition of PANI from leucoemeraldine (semiconducting state) to emeraldine form (conducting sate) while peaks (C_2/A_2) are ascribed to the transformation from emeraldine to pernigraniline.[25, 26] PANI-RGO-MWNTs ternary film exhibits larger current density response compared to GO, PANI-GO and PANI-GO-MWNTs electrodes in the same scan rate, suggesting the ternary hybrid film has higher specific capacitance.

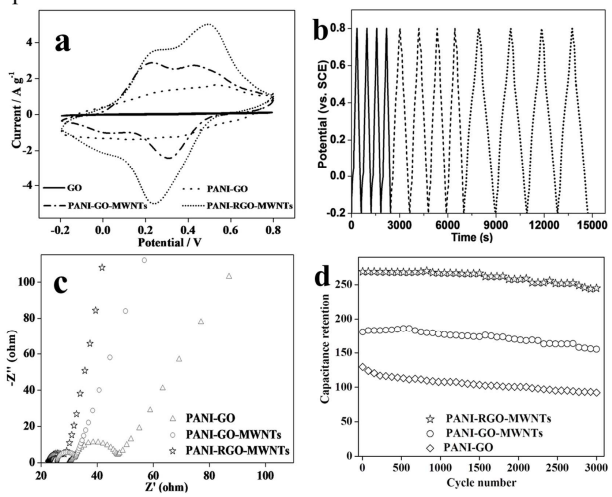

Fig. 8 (a) CV curves of MWNTs, PANI-GO, PANI-GO-MWNTs and PANI-RGO-MWNTs. (b) Continuous galvanostatic charge-discharge curves of PANI-RGO-MWNTs electrode at the current densities of 2 A g^{-1}, 1 A g^{-1} and 0.5 A g^{-1}. (c) Electrochemical impedance spectroscopy of the three electrodes. (d) Variation of the specific capacitance of three samples versus the cycle number.

The galvanostatic charge/discharges of PANI-RGO-MWNTs film electrode at different current densities were measured in 1 M H_2SO_4. As shown in Fig 8b, the charge-discharge curves keep similar shape at each four continuous cycles, which reveal that the ternary film can experience a wide range of current densities. PANI-RGO-MWNTs film electrode exhibits a high discharge/charge efficiency of 98.7% according to the ratio of the discharge time to the charge time, indicating excellent electrochemical reversibility and discharge/charge rate control capability. The specific capacitance of the electrode can be calculated from CV curves according to the equation $C_m = (I\Delta t)/(\Delta V m)$, where C_m is the specific capacitance, I is the constant discharge current, Δt is the discharge time, ΔV is the potential window, and m is the mass of the electroactive materials.[27] The specific capacitance of the PANI-RGO-MWNTs is about 498 F g^{-1} at 0.5 A g^{-1}. The greatly enhanced specific capacitance may result from the synergistic effect between RGO, MWNTs and PANI and the good electrical conductivity of the 3D conductive network synergistically assembled by MWNTs and RGO.

Fig. 8c exhibits the Nyquist diagrams of all examples, which all comsisit of a semicircle in the high frequency region and a straight line in the low frequency region, corresponding to the charge-transfer resistance of the electrode (R_{ct}) and the internal resistance (R_s),[28] respectively. R_{ct} is the diameter of the semicircle in real part of the sum resistance of the electrochemical system, which is one of the limiting factors for the power density of supercapacitors. In comparison to PANI-GO and PANI-GO-MWNTs electrodes, the R_{ct} of the PANI-RGO-MWNTs electrode reduces remarkably due to the formation of 3D conductive network by the use of MWNTs to bridge the gaps between RGOs. The low resistance of the PANI-RGO-MWNTs electrode makes it possible for high power performance flexible supercapacitor.

For further understanding of the electrochemical performances, the long-term cycle life of the electrodes was also evaluated in our work by repeating the CV test at a scan rate of 50 mV s^{-1}. The specific capacitance as a function of the cycle number is presented in Fig. 8d. It is found that the PANI-RGO-MWNTs electrode exhibits excellent long cycle life. After 3000 cycles, the capacitance retained 95.8% of initial capacitance compared to to 94.2% for PANI-GO-MWNTs electrode and 93.3% for PANI-GO electrode, demonstrating that PANI-RGO-MWNTs electrode exhibits excellent cycle stability and a very high degree of reversibility in the repetitive scan cycle. The improved cycle stability is primarily attributed to the extraordinary electrical conductivity of PANI-RGO-MWNTs electrode originated from the formation of 3D conductive network by introduction of MWNTs into RGO system. Therefore, this ternary hybrid film has great potential applications in flexible supercapacitors.

According to the aboved results of electrochemical performance, the good energy storage characteristics of the PANI-RGO-MWNTs flexible film are main attributed to two aspects. Except for their special synergistic effect of three components, which combine the good redox property of PANI with high conductivity of MWNTs and RGO. The excellent performance of ternary hybrid film also depends on the novel

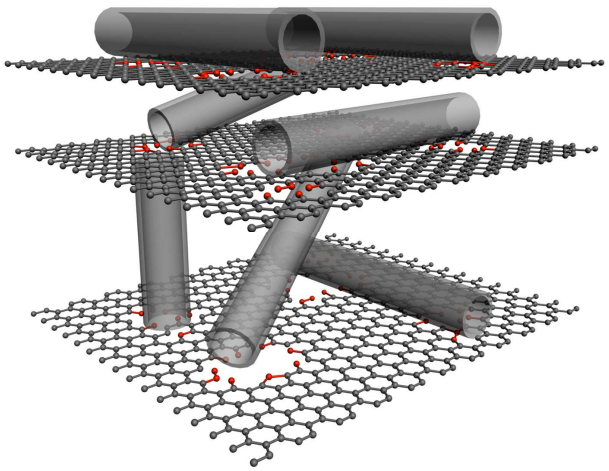

Fig. 9 Schematic representation of the superiority of the 3D conductive network using MWNTs to bridge the defect of RGO for fast ion transport.

3D conductive network of RGO bridging by MWNTs (Figure 9). As we known, GO after reduction is extremely defective in comparison to the high quality of graphene cleaved directly from graphite. Hence the conductivity of RGO is far below the conductivity of graphene. In this paper, we successfully introduce MWNTs into GO system, which effectively increase the basal spacing between GO sheets. Even more important, MWNTs insert into the layers of GO sheets, serving as a bridge to connect the defects induced by reduction GO (the defects in a single-layer graphene or adjacent layers). This is conductive to form a 3D conductive network for the efficient electron transfer, which endows rapid transport of the electrolyte ions and electrons throughout the electrode matrix, reducing the internal resistance of the electrode to result in the comprehensive utilization of pseudo- capacitance and double-layer capacitance. Thus, the high performance ternary flexible supercapacitor can be expected based on this 3D conductive network.

Conclusions

In summary, 3D conductive network supported free-standing PANI-RGO-MWNTs hybrid film has been designed and prepared by a simple rapid-mixture polymerization. The obtained ternary hybrid films maintain the pristine flexibility of GO-MWNTs film and display highly electrochemical performances due to the remarkable combination of advantages coming from the synergistic effect between MWNTs, RGO and PANI, and more importantly, MWNTs serve as a bridge to connect the defects of RGO to form a 3D conductive network to enhance the efficient electron transfer. Thus, the high performance ternary flexible supercapacitor can be designed and prepared simply based on this 3D conductive network, making such film-like hybrid papers promising flexible electrode materials for various applications in the electrochemical energy storage, such as flexible supercapacitors and batteries.

Acknowledgements

This work was supported by the National Natural Science Foundation of China (NSFC) (Grant No. 21121001), the Ministry of Science and Technology (2009CB930404). Shenzhen Science and Technology Research Grant (No. ZDSY20130331145131323, CXZZ20120829172325895, JCYJ20120614150338154). We acknowledge Beijing Municipal Commission of Education for the special fund for the Disciplines & Postgraduate Education Construction Project.

Notes and references

[a] *School of Advanced Materials, Peking University Shenzhen Graduate School, Shenzhen 518055, P.R. China Tel&Fax: 86-755-26033200; E-mail: panfeng@pkusz.edu.cn*

[b] *Beijing National Laboratory for Molecular Sciences, Laboratory of Polymer Physics and Chemistry, Institute of Chemistry, Chinese Academy of Sciences, Beijing 100190, P. R. China. E-mail: zhaoning@iccas.ac.cn, jxu@iccas.ac.cn*

1. M. Winter and R. J. Brodd, *Chem. Rev.*, 2004, **104**, 4245.
2. M. Armand and J. M. Tarascon, *Nature*, 2008, **451**, 652.
3. B. Kang and G. Ceder, *Nature*, 2009, **458**, 190.
4. H. J. Lin, L. Li, J. Ren, Z. B. Cai, L. B. Qiu, Z. B. Yang and H. S. Peng, *Sci. Rep.*, 2013, **3**, 1353.
5. Z. Niu, P. Luan, Q. Shao, H. Dong, J. Li, J. Chen, D. Zhao, L. Cai, W. Zhou, X. Chen, S. Xie, *Energy Environ. Sci.*, 2012, **5**, 8726.
6. D. W. Wang, F. Li, J. P. Zhao, W. C. Ren, Z. G. Chen, J. Tan, Z. S. Wu, I. Gentle, G. Q. Lu and H. M. Cheng, *ACS Nano*, 2009, **3**, 1745.
7. L. Ji, Z. Lin, A. J. Medford and X. Zhang, *Carbon*, 2009, **47**, 3346.
8. E. J. Ra, E. Raymundo-Piñero, Y. H. Lee and F. Béguin, *Carbon*, 2009, **47**, 2984.
9. X. Chen, L. Qiu, J. Ren, G. Guan, H. Lin, Z. Zhang, P. Chen, Y. Wang and H. Peng, *Adv. Mater.*, 2013, **25**, 6436.
10. J. Ren, W. Bai, G. Guan, Y. Zhang and H. Peng, *Adv. Mater.*, 2013, **25**, 5965.
11. Q. Wang, J. Yan, Z. Fan, T. Wei, M. Zhang and X. Jing, *J Power Sources*, 2014, **247**, 197.
12. C. Meng, C. Liu, L. Chen, C. Hu and S. Fan, *Nano Letters*, 2010, **10**, 4025.
13. L. Huang, B. Wu, G. Yu and Y. Liu, *J. Mater. Chem.*, 2011, **21**, 919.
14. C. Meng, C. Liu and S. Fan, *Electrochem. Commun.*, 2009, **11**, 186.
15. Q. Wu, Y. Xu, Z. Yao, A. Liu and G. Shi, *ACS Nano*, 2010, **4**, 1963.
16. L. L. Zhang, R. Zhou and X. S. Zhao, *J. Mater. Chem.*, 2010, **20**, 5983.
17. X. Fang, Z. Yang, L. Qiu, H. Sun, S. Pan, J. Deng, Y. Luo and H. Peng, *Adv. Mater.*, 2014, **26**, 1694.
18. Z. Yang, M. Liu, C. Zhang, W. W. Tjiu, T. Liu and H. Peng, *Angew. Chem. In.t Ed.*, 2013, **52**, 3996.
19. Z. Fan, J. Yan, L. Zhi, Q. Zhang, T. Wei, J. Feng, M. Zhang, W. Qian and F. Wei, *Adv. Mater.*, 2010, **22**, 3723.
20. N. I. Kovtyukhova, P. J. Ollivier, B. R. Martin, T. E. Mallouk, S. A. Chizhik, E. V. Buzaneva and A. D. Gorchinskiy, *Chem. Mater.*, 1999, **11**, 771.
21. S. Pei, J. Zhao, J. Du, W. Ren and H. M. Cheng, *Carbon*, 2010, **48**, 4466.
22. X. B. Yan, J. T. Chen, J. Yang, Q. J. Xue, P. Miele, *ACS Appl. Mater. Interfaces*, 2010, **2**, 2521.
23. R. V. Salvatierra, M. M. Oliveira and A. J. G. Zarbin, *Chem. Mater.*, 2010, **22**, 5222
24. X. Lu, H. Dou, B. Gao, C. Yuan, S. Yang, L. Hao, L. Shen, X. Zhang, *Electrochim. Acta*, 2011, **56**, 5115.
25. J. Wei, J. Zhang, Y. Liu, G. Xu, Z. Chen, Q. Xu, *RSC Adv.*, 2013, **3**, 3957.
26. C. C. Hu, J. Y. Lin, *Electrochim. Acta,* 2002, **47**, 4055.
27. H. Fan, H. Wang, N. Zhao, X. Zhang and J. Xu, *J. Mater. Chem.*, 2012, **22**, 2774.
28. Y. Q. Dou, Y. P. Zhai, H. J. Liu, Y. Y. Xia, B. Tu, D. Y. Zhao and X. X. Liu, *J. Power Sources*, 2011, **196**, 1608.